Desalination and Water Treatment
www.deswater.com

doi: 10.5004/dwt.2019.24765

171 (2019) 158–163
December

Highly efficient solar light-assisted copper decorated zinc oxide nanocomposites for photocatalytic reduction of mercury

A.S. Basaleh

Department of Chemistry, Faculty of Science, King Abdulaziz University, P.O. Box: 80203, Jeddah 21589, Saudi Arabia, Tel. +966-126400000; email: amalbasaleh1@gmail.com

Received 21 April 2019; Accepted 31 July 2019

ABSTRACT

A modified sol-gel route was used to prepare zinc oxide nanorods, and its sample was named as the Z sample. Photoassisted-deposition regime has been utilized to decorate ZnO nanorods with copper; percentage weight of Cu dopant was adjusted to be 0.3, 0.6, 0.9 and 1.2 wt.%, their samples were named as CuZ-0.3, CuZ-0.6, CuZ-0.9 and CuZ-1.2 samples, respectively. Z and CuZ samples were characterized using different tools. The values of the surface area of Z, CuZ-0.3, CuZ-0.6, CuZ-0.9 and CuZ-1.2 samples are 80, 78, 76, 73 and 70 m^2/g, respectively. Thus, decoration of copper in zinc oxide surface blocks some pore of zinc oxide and hence reduces surface area. XPS results reveal that copper was decorated in zinc oxide nanorods surface as metallic copper. The efficiency of Z and CuZ samples was inspected for the reduction of mercury ions under visible light. Photocatalyst of CuZ-0.9 sample has the best photocatalytic activity for reduction of mercury (II), at which 100% of mercury (II) can be reduced within 20 min using 0.9 g/L photocatalyst dose.

Keywords: Zinc oxide; Nanorods; Copper decoration; Reduction of mercury (II); Visible light

1. Introduction

Mercury can be used in different industries, for example electrical, electronic, and chlorine-alkali industry. Also, mercury can be used as catalysts in many technologies such as plastics, sulfonation, oxidation, chlorination, hydrogenation and dehydrogenation technology [1]. The central nervous system in both animals and humans has affected mercury compounds, so mercury compounds are very toxic compounds [2]. A lot of fisheries are infected by a high level of mercury, because of mercury inhalation vapor during fish consumption [3–5]. A mercury degradation rate by nature is extremely small. Thus, mercury must be degraded and removed. Many methods are used for removal of mercury, such as reduction and precipitation as sulfide, adsorption and ion exchange [1,6,7]. Newly, removal of mercury was carried out using photocatalysis process using photocatalyst as titanium dioxide [8–12]. In photocatalysis method, mercury (II) was reduced to metallic mercury by photogenerated electrons, which are created by irradiation of photocatalyst [10,12]. Also, the reduction of mercury (II), depends on both photocatalyst and source of irradiation [10,12]. The photocatalytic activity was increased in the presence of an organic scavenger, for example, citric acid, methanol and formic acid, due to reduced electron–hole recombination rate [13]. The commercial use of titanium dioxide as photocatalyst is delayed, due to its agglomeration and its absorption by UV light [14]. To overcome these two problems, a lot of ways were used. Doping of metals or non-metals is one of the methods to shift absorption of photocatalyst from UV region to visible region [15–28]. In this work, zinc oxide was prepared in nanorods shape to overcome zinc oxide agglomeration. The band gap of zinc oxide was reduced by the decoration of copper. The efficiency of Z and CuZ samples was inspected for the reduction of mercury ions under visible light.

2. Experimental

2.1. Preparation of zinc oxide nanorods

Arrangement A was set up by scattering zinc methoxide (0.2 mol) in a blend of methanol (0.5 mmol) and of tetraoctylammonium bromide (0.1 mmol) for 3 h sonication. On the other hand, arrangement B was set up by dissolution of acetic acid (0.1 mmol) in deionized water (30 mL). Arrangement B was mixed gradually to arrangement A utilizing via stirring at 30°C. The resultant precipitate was isolated, cleaned several times and left to dry under vacuum at 70°C for 10 h. After that, ZnO nanorods were accessed through firing the resultant precipitate at 400°C for 3 h.

2.2. Cu@ZnO nanocomposites preparation

Photo-assisted deposition regime has been utilized to decorate ZnO nanorods with copper; the percentage weight of Cu dopant was adjusted to be 0.3, 0.6, 0.9 and 1.2 wt.%. In this regime; ZnO nanorods solution and a solution of cupric acetate, as a copper metal origin, were subjected to UV light. All solutions were kept to dry overnight at about 100°C. Copper@ZnO nanorods could be obtained via H_2-reduction process (20 mL/min) for 2 h at 200°C.

2.3. Characterization

Morphology and microstructure for ZnO and Cu@ZnO nanorods were investigated via scanning electron microscope (JEOL-JSM-5410) as well as transmission electron microscopy (JEOL-JEM-1230). On the other hand, BET specific surface areas of the final materials were calculated utilizing A Nova 2000 series Chromatec instrument. A Bruker axis D8 X-ray diffraction was applied to investigate the phase composition of the resultant products (ZnO and Cu@ZnO nanorods) applying Cu Kα radiation of λ = 1.540 Å at ambient temperature. X-ray photoelectron spectroscopy was adopted to examine the state of the element. UV–Vis-NIR spectrophotometer (V-570, Jasco, Japan) was applied to investigate the band gap energies of the formed structures (ZnO and Cu@ZnO nanorods) at ambient temperature. Fluorescence spectrophotometer of Shimadzu RF-5301 type was administered to fix the photoluminescence emission spectra that required to recognize the e-h recombination rate.

2.4. Photocatalytic tests

The efficiency of the planned nanocomposites was inspected for the reduction of mercury ions. In this experiment, a certain weight of the photocatalyst was scattered by means of ultrasonic in 0.5 L of $HgCl_2$ solution (100 ppm Hg (II) was applied as a starting dose). 500-W Xenon lamp arisen on a photocatalytic reactor was adopted to produce artificial Vis light which illuminates the reaction mixture. A cutoff filter with λ > 420 nm was applied as well as a water tube was oppressed to avoid heating; this will enable constant temperature throughout the experiment (303 K). The quartz reactor was located at a distance of 11 cm away from the light origin. Previous to illumination, N_2 was introduced for 0.5 h in order to remove any dissolved O_2 from the solution. Each solution was illuminated for 1 h. After that, specimens were isolated from the reactor and permitted to centrifuge for 20 min at 7,000 rpm and filtrated to get rid of any undesired particles. The spectrophotometer that applied in band gap measurement was adopted to figure out the remaining Hg (II) after the reduction action.

3. Results and discussion

3.1. Characterization of materials

Fig. 1 shows XRD patterns for Z, CuZ-0.3, CuZ-0.6, CuZ-0.9 and CuZ-1.2 samples. The broad peaks at 31.8°, 34.5°, 36.3º, 47.6°, 56.7°, 62.9°, 67.0° and 68.1° suggest a zinc oxide phase structure for Z and CuZ samples. No peaks for copper or copper oxide were observed for the CuZ samples due to a high distribution of copper on the zinc-oxide surface. In addition, the reduction in the intensity of the characteristic peaks of the ZnO phase in the spectra for the CuZ samples suggests that the doping of copper decreases the crystallite sizes in the ZnO phase.

Fig. 2 shows SEM images for Z, CuZ-0.3, CuZ-0.6, CuZ-0.9 and CuZ-1.2 samples. Z, CuZ-0.3, CuZ-0.6, CuZ-0.9 and CuZ-1.2 samples show a nanorod shape. However, CuZ-0.3, CuZ-0.6, CuZ-0.9 and CuZ-1.2 samples are nanorods in shape and also covered by copper. It is clear that the addition of copper decreases the size of the ZnO nanorods.

Fig. 3a shows TEM image for the CuZ-0.9 sample. The CuZ-0.9 sample is nanorods in shape. The addition of copper to ZnO decreases the size of the ZnO sample and copper appears as a dot on the surface of the ZnO nanorods.

Fig. 3b shows the HRTEM image for the CuZ-0.9 sample. The presence of lattice spacing for (111) plane at 0.200 nm indicates that the copper is metallic copper. Also, the presence of lattice spacing for (002) plane at 0.262 nm indicates that the ZnO is present.

XPS spectra for Cu2p for the CuZ-0.9 sample are shown in Fig. 4. The presence of two binding peaks at 953.0 and 933.0 eV, for Cu2p 1/2 and Cu2p 3/2 indicate that the copper is metallic copper [29].

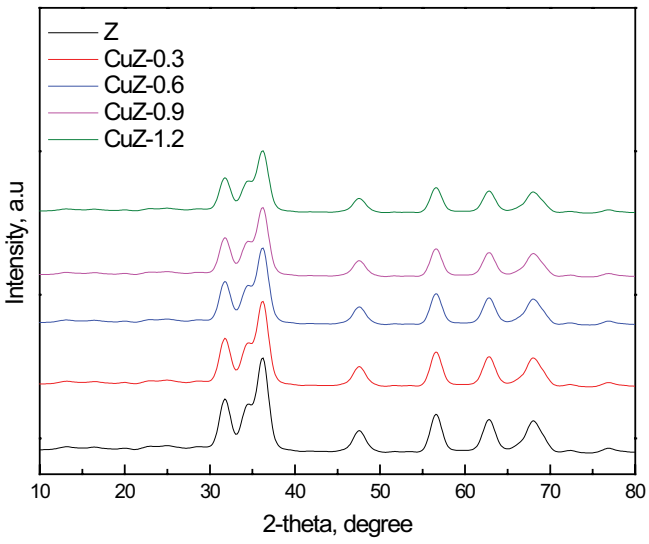

Fig. 1. XRD patterns for ZnO and Cu@ZnO samples.

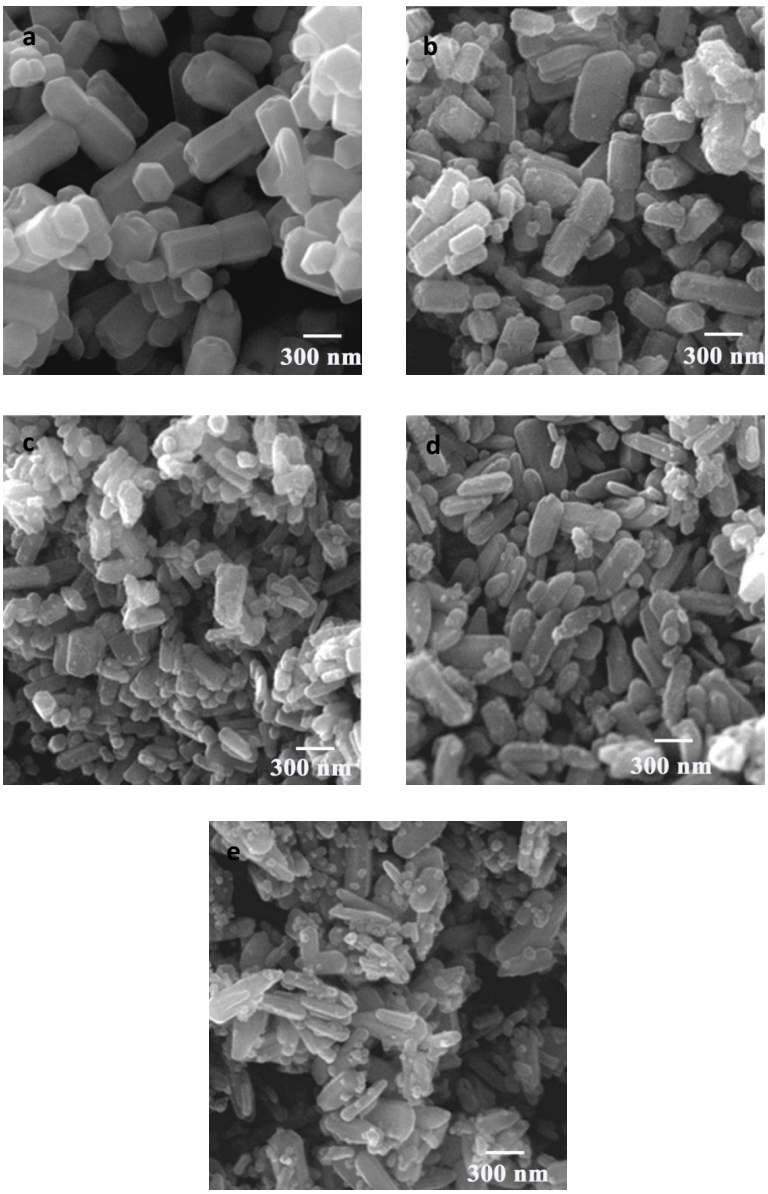

Fig. 2. SEM images for ZnO (a), 0.3 wt.% Cu@ZnO (b), 0.6 wt.% Cu@ZnO (c), 0.9 wt.% Cu@ZnO (d) and 1.2 wt.% Cu@ZnO (e) samples.

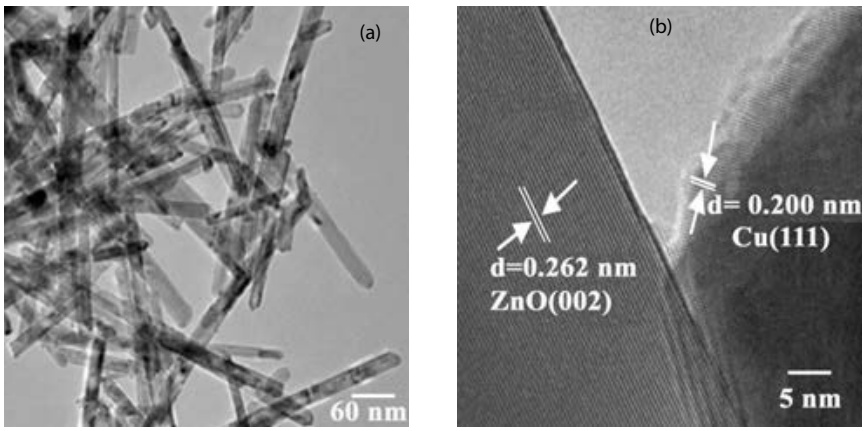

Fig. 3. (a) TEM image for the 0.9 wt.% Cu@ZnO and (b) HRTEM image for the 0.9 wt.% Cu@ZnO.

The specific surface area for the Z, CuZ-0.3, CuZ-0.6, CuZ-0.9 and CuZ-1.2 samples was measured. The values of the surface area of Z, CuZ-0.3, CuZ-0.6, CuZ-0.9 and CuZ-1.2 samples are 80, 78, 76, 73 and 70 m^2/g, respectively., as exposed in Table 1. Thus, decoration of copper in zinc oxide surface blocks some pore of zinc oxide and hence reduces surface area.

Fig. 5 shows the UV–Vis spectra for the Z, CuZ-0.3, CuZ-0.6, CuZ-0.9 and CuZ-1.2 samples. These data show that the ZnO absorbs in the UV region and that the addition of copper to the zinc-oxide nanorods leads to a shift in the absorption band for the zinc oxide from the ultraviolet region to the visible region. The values for the band gap energies were calculated using the UV–Vis spectra measured for the Z, CuZ-0.3, CuZ-0.6, CuZ-0.9 and CuZ-1.2 samples. The band gaps for the Z, CuZ-0.3, CuZ-0.6, CuZ-0.9 and CuZ-1.2 samples are 3.30, 2.90, 2.80, 2.68 and 2.67 eV, respectively as shown in Table 2.

Fig. 6 shows PL spectra for the Z, CuZ-0.3, CuZ-0.6, CuZ-0.9 and CuZ-1.2 samples. The Z sample shows a high PL peak intensity, with the addition of copper to the ZnO nanorods decreasing the position and intensity of the PL peak. The values for the band gap energies determined from the PL emission spectra measurements are found to be 3.31, 2.91, 2.81, 2.69 and 2.68 eV for the Z, CuZ-0.3, CuZ-0.6, CuZ-0.9 and CuZ-1.2 specimens, respectively. These values are very close to those obtained from the UV–Vis spectra as discussed in the previous paragraph.

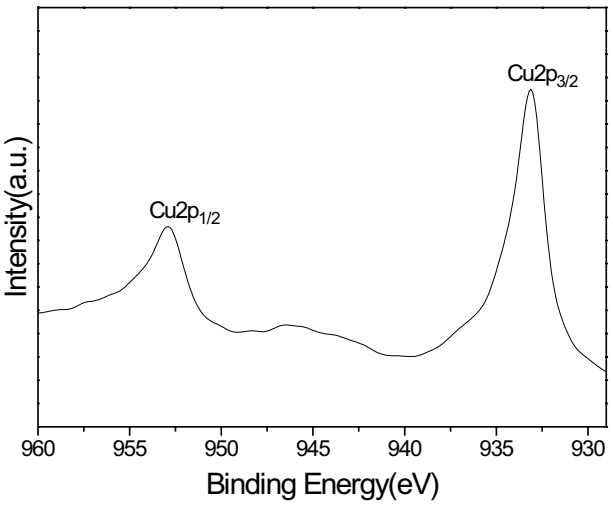

Fig. 4. XPS spectra for Cu2p in the 0.9 wt.% Cu@ZnO sample.

Table 1
BET surface area of ZnO and Cu@ZnO samples

Sample	S_{BET} (m^2/g)
Z	80
CuZ-0.3	78
CuZ-0.6	76
CuZ-0.9	73
CuZ-1.2	70

3.2. Photocatalytic performance

As mentioned earlier, the reduction of the mercury ion was utilized to test the synthesized photocatalyst. Fig. 7 shows the effect of the copper weight percentage on the mercury-ion reduction. The photocatalytic reduction of the mercury ion with use of the Z sample is very small (3%); this can be explained by the fact that the Z sample absorbs only in the UV region while the light source used covers the visible region. The photocatalytic reduction of the mercury ion with use of the CuZ-0.3, CuZ-0.6, CuZ-0.9 and CuZ-1.2 samples were at 45%, 80%, 100% and 100%, respectively. It is obvious that the inclusion of Cu enhances the reduction reaction of the mercury ion applying the photocatalyst. The CuZ-0.9 sample exhibits superior efficiency with an approximately 100% conversion within 60 min.

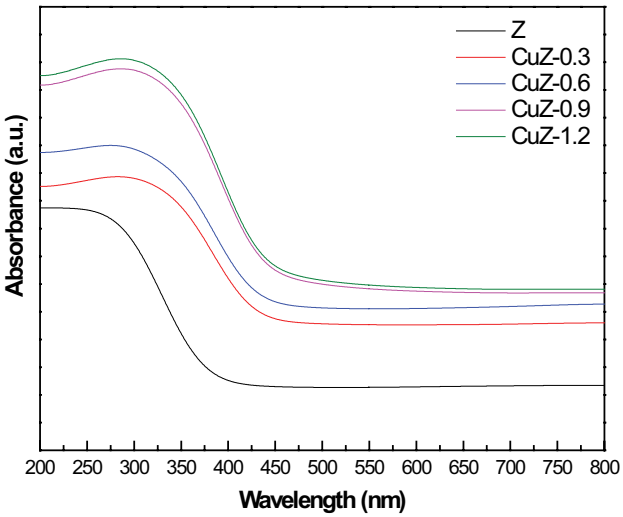

Fig. 5. UV–Vis spectra for the ZnO and Cu@ZnO samples.

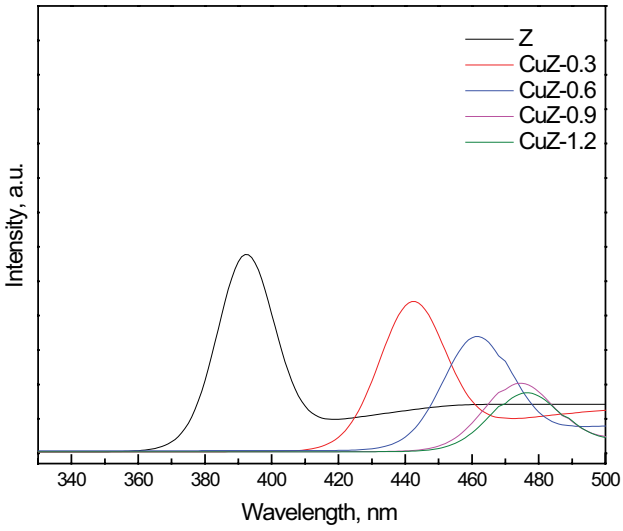

Fig. 6. PL spectra for the ZnO and Cu@ZnO samples.

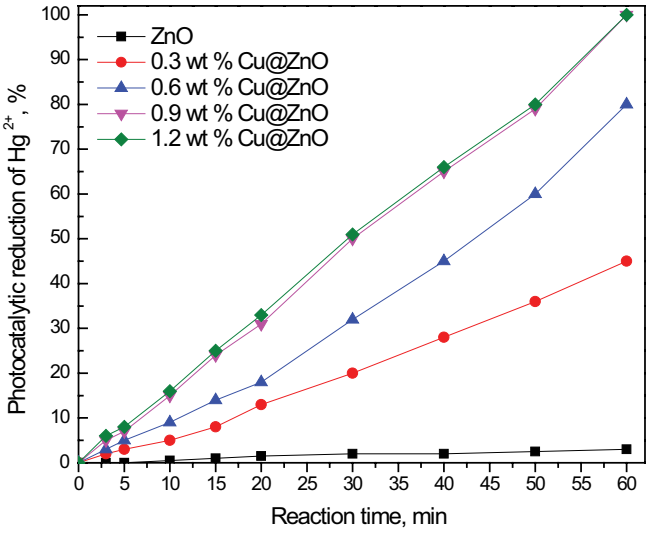

Fig. 7. Effect of varying the weight percentage of copper on photocatalytic reduction of the mercury ion.

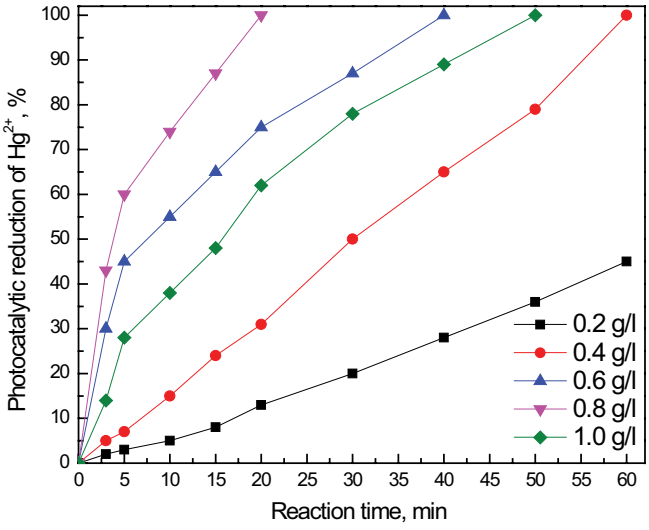

Fig. 8. Effect of the dose of the 0.9 wt.% Cu@ZnO photocatalyst for photocatalytic reduction of the mercury ion.

The effect of the amount of catalyst added to the reaction was also studied. Fig. 8 shows the effect of the dose of the CuZ-0.9 photocatalyst on the photocatalytic reduction of the mercury ion. By increasing the dose from 0.2 to 0.4 g/L, the photocatalytic reduction of the mercury ion increased from 45% to 100%, respectively. By increasing the dose of the CuZ-0.9 photocatalyst from 0.4 to 0.8 g/L, the reaction time required for a complete photocatalytic reduction of the mercury ion decreased from 60 to 20 min, respectively. This may be due to an increased number of available active sites due to the increased photocatalyst dose. If the dose was raised above 0.8 g/L to a value of 1.0 g/L, the reaction time required for complete photocatalytic reduction of the mercury ion increased from 20 to 50 min. Increasing the dose of the photocatalyst beyond a certain point may

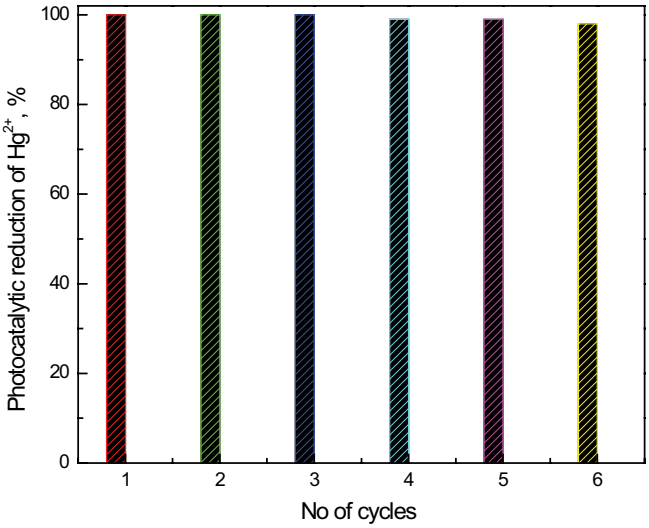

Fig. 9. Recycling and reuse of the 0.9 wt.% Cu@ZnO photocatalyst for photocatalytic reduction of the mercury ion.

Table 2
Band gap energy of ZnO and Cu@ZnO samples

Sample	SBET (m^2/g)
Z	3.30
CuZ-0.3	2.90
CuZ-0.6	2.80
CuZ-0.9	2.68
CuZ-1.2	2.67

hinder the penetration of light to reach all the active sites on the photocatalyst.

A test for the possibility of the reuse of the catalyst was also performed. Fig. 9 shows the recycling and reuse of the CuZ-0.9 photocatalyst for the photocatalytic reduction of the mercury ion. This figure shows that the photocatalytic reduction of the mercury ion remains constant even if the catalyst is reused five times, indicating great stability for the CuZ-0.9 photocatalyst.

4. Conclusions

Uniform Z and CuZ nanorods samples were produced by a sol-gel method. The reduction of mercury ions was utilized to test the synthesized photocatalysts under visible light. The values for the specific surface area of the Z, CuZ-0.3, CuZ-0.6, CuZ-0.9 and CuZ-1.2 samples are 80, 78, 76, 73 and 70 m^2/g, respectively, which indicates that the Z sample shows a higher BET surface area compared with the CuZ samples. The Z and CuZ samples show a nanorods shape, as determined by TEM. The photocatalytic performance for the nanocomposites was studied by mercury (II) reduction under visible light. In terms of photocatalytic performance for mercury (II) reduction, CuZ-0.9 outperforms CuZ-0.6 by 1.25 times, CuZ-0.3 by 2.22 times and Z by 33.3 times.

References

[1] W.J. Patterson, Wastewater Treatment Technology, Ann Arbor Science, Michigan, 1975.
[2] R.D. Cassidy, A. Furr, Toxicity of Heavy Metals in the Environment, Part 1 (Edited by F. W. Oehme),.Marcel Dekker, New York, 1978.
[3] U.S. E.P.A., Mercury Study Report to Congress, EPA-425/R-97-006, Office of Air Quality Planning & Standards and Office of Research and Development, 1997.
[4] F. Zahir, S.J. Rizwi, S.K. Haq, R.H. Khan, Low dose mercury toxicity and human health, Environ. Toxicol. Pharmacol., 20 (2005) 351–360.
[5] U.N.E.P. Chemicals, Global Mercury Assessment, Report no. 54790-01, Geneva, Switzerland, 2002.
[6] J.M. Hammer, Water and Wastewater Technology, Wiley, New York, 1975.
[7] A. Pamalho, Introduction to Wastewater Treatment Processes. Academic Press, London, 1977.
[8] N. Serpone, K. Ah-You, T.P. Tran, R. Harris, AM1 simulated sunlight photoreduction and elimination of Hg(II) and CH3Hg(II) chloride salts from aqueous suspensions of titanium dioxide, Sol. Energy, 39 (1987) 491–498.
[9] M.A. Aguado, S. Cervera-March, J. Gimenez, Continuous photocatalytic treatment of mercury(II) on titania powders: kinetics and catalyst activity, Chem. Eng. Sci., 50 (1995) 1561–1569.
[10] S.G. Botta, D.J. Rodriguez, A.G. Leyva, M.I. Litter, Features of the transformation of Hg-II by heterogeneous photocatalysis over TiO_2, Catal. Today, 76 (2002) 247–258.
[11] L.B. Khalil, M.W. Rophael, W.E. Mourad, The removal of the toxic Hg(II) salts from water by photocatalysis, Appl. Catal. B, 36 (2002) 125–130.
[12] X. Wang, S.O. Pehkonen, A.K. Ray, Photocatalytic reduction of Hg(II) on two commercial TiO_2 catalysts, Electrochim. Acta, 49 (2004) 1435–1444.
[13] U.S. E.P.A., Water Quality Criterion for the Protection of Human Health: Methyl mercury, EPA-823-R-01-001, Office of Science and Technology and Office of Water, 2001.
[14] J. Aguado, R. van Grieken, M. Lopex-Munoz, J. Marugan, A comprehensive study of the synthesis, characterization and activity of TiO_2 and mixed TiO_2/SiO_2 photocatalysts, Appl. Catal. A, 312 (2006) 202–212.
[15] C. Anderson, A.J. Bard, Improved photocatalytic activity and characterization of mixed TiO_2/SiO_2 and TiO_2/Al_2O_3 materials, J. Phys. Chem. B, 101 (1997) 2611–2616.
[16] K.Y. Jung, S.B. Park, Enhanced photoactivity of silica-embedded titania particles prepared by sol–gel process for the decomposition of trichloroethylene, Appl. Catal. B, 25 (2000) 249–256.
[17] P. Pucher, M. Benmami, R. Azouani, G. Krammer, K. Chhor, J.F. Bocquet, A.V. Kanaev, Nano-TiO_2 sols immobilized on porous silica as new efficient photocatalyst, Appl. Catal. A, 332 (2007) 297–303.
[18] E. Pitoniak, C.Y. Wu, D. Londeree, D. Mazyck, J.C. Bonzongo, K. Powers, W. Sigmund, Nanostructured silica-gel doped with TiO_2 for mercury vapor control, J. Nanopart. Res., 5 (2003) 281–292.
[19] H.E. Byrne, W.L. Kostedt, J.M. Stokke, D.W. Mazyck, Characterization of HF catalyzed silica gels doped with Degussa P25 titanium dioxide, J. Non-Cryst. Solids, 355 (2009) 525–530.
[20] E. Pitoniak, C.Y. Wu, D.Q. Mazyck, K.W. Powers, W. Sigmund, Adsorption enhancement mechanisms of silica–titania nanocomposites for elemental mercury vapor removal, Environ. Sci. Technol., 39 (2005) 1269–1274.
[21] J.M. Stokke, D.W. Mazyck, Development of a regenerable system employing silica–titania composites for the recovery of mercury from end-box exhaust at a chlor-alkali facility, J. AirWaste Manage. Assoc., 58 (2008) 530–537.
[22] J.M. Stokke, D.W. Mazyck, C.Y. Wu, R. Sheahan, Photocatalytic oxidation of methanol using silica–titania composites in a packed-bed reactor, Environ. Prog., 25 (2006) 312–318.
[23] J.L. Parker, N.S. Bloom, Preservation and storage techniques for low-level aqueous mercury speciation, Sci. Total Environ., 337 (2005) 253–263.
[24] A. Kanta, R. Sedev, J. Ralston, Thermally and photoinduced changes in the water wettability of low-surface-area silica and titania, Langmuir, 21 (2005) 2400–2407.
[25] A. Kanta, R. Sedev, J. Ralston, Preparation of silica-on-titania patterns with a wet ability contrast, Langmuir, 21 (2005) 5790–5794.
[26] H. Zhang, Photochemical redox reactions of mercury, Struct. Bond., 120 (2006) 37–79.
[27] C. Tian, Q. Zhang, A. Wu, M. Jiang, Z. Liang, B. Jiang, H. Fu, Cost-effective large-scale synthesis of ZnO photocatalyst with excellent performance for dye photodegradation, Chem. Commun., 48 (2012) 2858–2860.
[28] B. Li, T. Liu, Y. Wang, Z. Wang, ZnO/ graphene-oxide nanocomposite with remarkably enhanced visible-light-driven photocatalytic performance, J. Colloid Interface Sci., 377 (2012) 114–121.
[29] Aramice Y.S. Malkhasian, Reda M. Mohamed, Environmental remediation of Cr(VI) solutions by photocatalytic reduction using Ag-$Er(OH)_3$ nanocomposite, J. Alloys Comp., 632 (2015) 735–740.